PERGAMON

Vision Research 39 (1999) 445–465

Vision Research

Position jitter and undersampling in pattern perception

Dennis M. Levi [a,*], Stanley A. Klein [b], Vineeta Sharma [a]

[a] College of Optometry, University of Houston, Houston, TX 77204-6052, USA
[b] School of Optometry, University of California at Berkeley, Berkeley, CA 94720, USA

Received 3 December 1997; received in revised form 9 April 1998

Abstract

The present paper addresses whether topographical jitter or undersampling might limit pattern perception in foveal, peripheral and strabismic amblyopic vision. In the first experiment, we measured contrast thresholds for detecting and identifying the orientation (up, down, left, right) of E-like patterns comprised of Gabor samples. We found that detection and identification thresholds were both degraded in peripheral and amblyopic vision; however, the orientation identification/detection threshold ratio was approximately the same in foveal, peripheral and amblyopic vision. This result is somewhat surprising, because we anticipated that a high degree of uncalibrated topographical jitter in peripheral and amblyopic vision would have affected orientation identification to a greater extent than detection. In the second experiment, we investigated the tolerance of human and model observers to perturbation of the positions of the samples defining the pattern when its contrast was suprathreshold, by measuring a 'jitter threshold' (the amount of jitter required to reduce performance from near perfect to 62.5% correct). The results and modeling of our jitter experiments suggest that pattern identification is highly robust to positional jitter. The positional tolerance of foveal, peripheral and amblyopic vision is equal to about half the separation of the features and the close similarity between the three visual systems argues against extreme topographical jitter. The effects of jitter on human performance are consistent with the predictions of a 'template' model. In the third experiment we determined what fraction of the 17 Gabor samples are needed to reliably identify the orientation of the E-patterns by measuring a 'sample threshold' (the proportion of samples required for 62.5% correct performance). In foveal vision, human observers are highly efficient requiring only about half the samples for reliable pattern identification. Relative to an ideal observer model, humans perform this task with 85% efficiency. In contrast, in both peripheral vision and strabismic amblyopia more samples are required. The increased number of features required in peripheral vision and strabismic amblyopia suggests that in these visual systems, the stimulus is underrepresented at the stage of feature integration. © 1998 Elsevier Science Ltd. All rights reserved.

Keywords: Amblyopia; Peripheral vision; Undersampling; Positional uncertainty; Psychophysics; Ideal-observer; Modeling

1. Introduction

The human visual system is able to effortlessly integrate local features to form our rich perception of patterns. Visual information is discretely sampled by the retina and cortex, and, at least at the early stages of visual processing, the normal visual system displays a highly ordered topographical mapping of visual information from retina to cortex. In normal foveal vision, the image is densely sampled, and the topographical mapping is very precise, enabling us to accurately preserve spatial relationships among objects or their constituent features. However, in peripheral vision, and in the fovea of strabismic amblyopes, spatial vision is degraded. There are three general classes of explanation for the degradation of peripheral and strabismic amblyopic vision: (i) a shift in the spatial scale of analysis as a consequence of reduced contrast sensitivity at high spatial frequencies (Levi & Waugh, 1994; Levi, Waugh & Beard, 1994); (ii) a reduced retinal and/or cortical sampling density (undersampling) (Levi & Klein, 1985, 1986; Levi, Klein & Yap, 1987; Wilson, 1991; Levi, Klein & Wang, 1994a,b; Levi & Klein, 1996); and (iii) topographical disorder (jitter) of cortical receptive fields which is uncalibrated (Hess, Campbell & Greenhalgh, 1978; Levi & Klein, 1985; Watt & Hess, 1987; Hess & Watt, 1990; Wilson, 1991; Hess & Field, 1994; Field & Hess, 1996). An extreme version of this jitter hypothesis suggests that in peripheral (and amblyopic) vision, the

* Corresponding author. Fax: +1 713 7431888; e-mail: dlevi@uh.edu.

0042-6989/98/$ - see front matter © 1998 Elsevier Science Ltd. All rights reserved.
PII: S0042-6989(98)00125-4

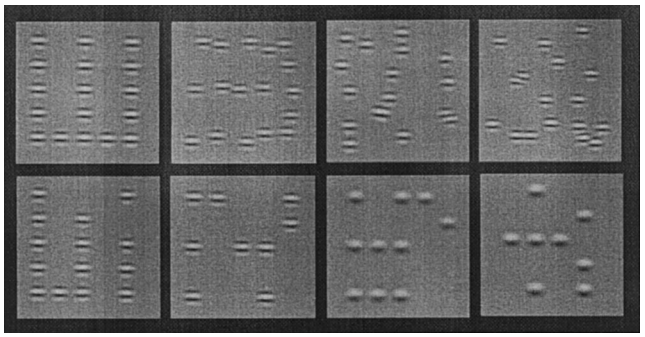

Fig. 1. Top row: examples of our E-like pattern showing (from left to right) increasing Gaussian jitter. The patches contain one carrier cycle per envelope standard deviation. Bottom row: 'undersampled' E's showing (from left to right) increasing 'undersampling'. The left two panels have one carrier cycle per envelope standard deviation, the right two have 0.5 carrier cycles per envelope standard deviation.

jitter may be larger than the receptive field (Hess & Field, 1993, 1994), and that there may actually be cross-overs (or swaps in the ordering) of information as it is transferred up through the visual nervous system (Hess & McCarthy, 1994).

The evidence in favor of topographical jitter comes mainly from experiments showing that position information is severely degraded in peripheral and amblyopic vision, while contrast discrimination is not (Hess & Field, 1994; Levi, Klein and Wang, 1994b; Field & Hess, 1996; Levi & Klein, 1996). Extreme topographical jitter would be very disruptive for pattern perception. Consider the E-like patterns in Fig. 1, which was constructed from 17 circular Gabor 'samples'. Jittering the positions of the samples would be expected to interfere with identification of the orientation of the pattern, but it should have little effect on the threshold for detection of the pattern.

The present paper addresses whether topographical jitter or undersampling might limit pattern perception in foveal, peripheral and strabismic amblyopic vision. In the first experiment, we measure contrast thresholds for detecting and identifying the orientation of patterns like that shown in Fig. 1. There is a straightforward prediction of the extreme jitter hypothesis—if there is a large amount of uncalibrated positional jitter in peripheral or amblyopic vision, then thresholds for identifying the orientation of the pattern should be degraded more than thresholds for detecting the pattern. In the second and third experiments, we investigated the tolerance to perturbation of the positions and numbers of the samples defining the pattern when its contrast was suprathreshold. Finally, we explore computational models of jitter and undersampling. To anticipate, our results and modeling suggest that pattern identification is rather robust to positional jitter. Pattern identification can tolerate position jitter of about half the separation of the features in foveal, peripheral and amblyopic vision. The close similarity between the three visual systems argues against extreme topographical jitter in amblyopic and peripheral vision. Pattern identification can tolerate undersampling of about half the samples in normal fovea; however, both peripheral and strabismic amblyopic vision require more samples. The increased number of samples required in peripheral vision and strabismic amblyopia suggests that in these visual systems, the stimulus is underrepresented at the stage of feature integration.

2. Methods

2.1. Stimuli

Our stimuli were E-shaped patterns. We chose E-shaped patterns because, like letters, these patterns are very familiar (even 'overlearned'); they are closely similar to the optotypes that are used in clinical acuity testing (sometimes referred to as 'illiterate E's'); and as described in Appendix A, human performance can be compared to an ideal observer model. The E-shaped patterns were composed of 17 circular Gabor patches (i.e. the luminance distribution of each element is described by the product of a circular Gaussian and an oriented sinusoid) and were displayed on either a Mitsubishi diamond scan 20H or a 21TX monitor via a Cambridge research systems VSG 2 graphics card with a resolution of 1152×960 pixels. The monitor frame rate was 72 Hz. The mean luminance of the display area was 56 cd/m^2. Gamma correction was applied using one of five palettes of 256 gray levels from a possible 4096 gray levels. The dynamic range and gray level increment was adjusted so that for the low contrast stimuli used in our study, the smallest contrast step size was on the order of 0.05%.

In our experiments, each Gabor patch had a Gaussian envelope with a standard deviation (σ) fixed at either 14 pixels or 28 pixels, and the envelope was truncated at $\pm 1.5\,\sigma$ (i.e. full width 3σ), and unless otherwise specified, the patches were abutting (i.e. they had a center-to-center separation equal to 3σ. The sinusoidal carrier was always horizontal, in sine phase, and had a spatial period of either $N = 1$ or 0.5 c/σ, resulting in a spatial frequency full bandwidth (specified at half the peak amplitude) of 0.55 or 1.1 octaves (the spatial frequency full bandwidth is approximately $0.55/N$ octaves, where N is the number of cycles/σ) (Levi & Klein, 1992). In order to evaluate performance over a wide range of stimulus conditions, we varied the observers' viewing distance, while keeping the screen dimensions of the stimuli constant (unless otherwise stated). Thus, at each viewing distance, the stimuli were scaled replicas.

2.2. Observers

Three observers with normal visual acuity (two of the

Table 1
Visual characteristics of amblyopes

OBS	Age	Sex	Eye	Rx	Acuity[a]	Fixation[b]	Strabismus
RH	32	M	OD	$-1.00/-0.50\times170$	20/15	Central	
			OS	$-1.50-1.50\times10$	20/36	Unsteady	Microtropia L. ET., 2^{Δ}
AJ	27	F	OD	$+5.50/-2.50\times20$	20/60	1.5^{0} Temporal	Constant R. XT., 4^{Δ}
			OS	-0.25	20/15	Central	
JB	40	M	OD	$+1.75/-0.50\times142$	20/38	0.5 Nasal	Constant R. ET., 6^{Δ}
			OS	$+1.25/-1.0\times25$	20/20	Central	
DM	39	F	OD	$-0.50/-0.25\times92$	20/20	Central	
			OS	$+2.50/-1.0\times160$	20/70	0.5^{0} Nasal	Constant L. XT., 3^{Δ}
CB	37	M	OD	$+4.25$	20/15	Central	
			OS	$-9.75/-0.75\times140$	20/200	$0.75–1^{0}$ Nasal	Constant L. ET., 4^{Δ}
DS	22	M	OD	$-0.25/-0.25\times90$	20/15	Central	
			OS	$+7.25/-0.5\times160$	20/101	Unsteady ($\approx 0.25°$ sup)	Constant L. XT., 6^{Δ}

[a] 75% correct on Davidson-Eskridge charts.
[b] Fixation determined with Haidinger's brushes and visuoscopy.

authors, and one naive as to the purpose of the experiments) and six observers with strabismic amblyopia (see Table 1 for details) served as observers. For all observers, viewing was monocular, with the untested eye occluded with a black patch. All observers were well practiced in making psychophysical judgments.

2.3. Experiment 1: Detection and identification of the orientation of an E-pattern

The purpose of the first experiment was to evaluate whether the raised levels of uncalibrated jitter thought to be resident in the normal periphery and in the central field of strabismic amblyopes, interferes more with identification of the orientation of the pattern, than with detection of the pattern. Thus, in this experiment, we measured contrast thresholds for both orientation identification and for detection.

2.3.1. Orientation identification

On each trial, the E-pattern was flashed for 500 ms (accompanied by a tone) in one of four rotated orientations (up, down, left or right), and the observer's task was to identify the pattern orientation (i.e. a four-alternative forced-choice) by pressing one of four buttons indicating the orientation of the global pattern. Visual feedback was provided after each response.

Contrast thresholds for identifying the orientation of the E-pattern were estimated using the method of constant stimuli. Psychometric curves (with five near-threshold contrasts) were obtained for each stimulus condition, and contrast thresholds were estimated using a Weibull function. Each estimate, corresponding to the contrast resulting in 62.5% correct performance ($d' \approx 1.2$), was based on 125 trials. The contrast thresholds presented in Section 3 refer to the means of at least four individual threshold estimates.

2.3.2. Detection thresholds

Detection thresholds were determined using a two-alternative forced-choice procedure: an E-pattern at one of four rotated orientations was randomly presented in one of two temporal intervals of 500 ms (signaled by two tones with an interstimulus interval of 500 ms), and the observer's task was to report which interval contained the E-pattern (the non-target interval was a mean luminance blank field). Auditory feedback was provided after each response. The Gabor elements, their size and spacing, and the procedure for estimating contrast thresholds were identical to those for orientation identification, except that now the chance rate was 50% rather than 25%, and threshold was specified at 75% correct ($d' \approx 1.0$). In control experiments, we also measured the effects of jitter (described below) on identification and detection in the normal fovea.

2.4. Experiment 2: Jitter thresholds for identification of a suprathreshold E-pattern

In this experiment we determined the observer's tolerance to positional jitter by measuring 'jitter thresholds' for E-patterns of fixed suprathreshold contrast levels.

2.4.1. Jitter thresholds

To measure the 'jitter' thresholds, we subjected the two-dimensional positions of each feature to position jitter. We used two types of jitter, which gave equivalent results: annular jitter and two-dimensional Gaussian jitter. For the annular jitter, the radial distance of each sample from the unperturbed position was chosen from a one-dimensional Gaussian distribution whose mean was r and whose standard deviation[1], S.D. (in

[1] This unusual choice of standard deviation was the result of an initial programming error, with a happy outcome.

pixels) was $(r+2)/2\sqrt{3}$. For example, for $r=10$ pixels, the S.D. was $6/\sqrt{3}$. The angle of the displacement was chosen randomly from a uniform distribution between 0 and 359°. The method of constant stimuli was used to vary r, and threshold is defined as the radius, r, that reduces performance from near perfect to 62.5%. The advantage of this method over Gaussian jitter is that trials are not wasted at near-zero jitter levels. Control experiments using two-dimensional Gaussian jitter gave qualitatively and quantitatively similar results (Fig. 5A). In a given experimental run, the E-pattern was presented in one of four orientations, and the observer's task was to identify the orientation. Psychometric curves (with five levels of jitter) relating percent correct identification to the amount of jitter (either annulus radius, or Gaussian standard deviation) used for each stimulus condition, were fit with a Weibull function. An example of the psychometric curve relating percentage correct identification to jitter magnitude, averaged over many conditions, is shown in Fig. 12B. Each threshold estimate is based on 125 trials. The reported thresholds represent the mean of three to five individual threshold estimates.

2.5. Experiment 3: Sample thresholds for identification of a suprathreshold E-pattern

In this experiment we determined what fraction of the 17 Gabor samples are needed to reliably identify the orientation of the E-patterns.

2.5.1. Sample thresholds

We investigated the ability to interpolate the features into a pattern by varying the probability that each sample would be displayed (undisplayed samples were set to the mean luminance—see insets in Fig. 1) and measuring the 'sample threshold' (the proportion of samples required for 62.5% correct performance). Sample thresholds were measured and analyzed in the same way as the jitter thresholds, except that we varied the proportion of samples rather than jitter or contrast, from trial to trial. An example of the psychometric curve relating percentage correct identification to the sample probability, averaged over many conditions, is shown in Fig. 11B.

3. Results and discussion

3.1. Experiment 1: Detection and identification of the orientation of an E-pattern

Contrast thresholds are only slightly lower for detection than for orientation identification in foveal (Fig. 2 left panels, open symbols), peripheral (5° lower visual field, Fig. 2 left panels, solid symbols), and amblyopic (Fig. 3 left panels, solid symbols) vision. The left panels in Figs. 2 and 3 plot contrast thresholds for both detection (circles) and identification (triangles) as a function of the sample carrier spatial frequency. Note that since these data were obtained by varying the viewing distance, the angular Gaussian envelope size, and sample separation co-vary with spatial frequency. The righthand panels in Figs. 2 and 3 summarize the two key results. First, Figs. 2D and 3D show the well documented spatial frequency specific loss of contrast sensitivity in peripheral vision (Koenderink, Bouman & Bueno de Mesquita, 1978; Rovamo, Virsu & Nasanen, 1978; Virsu & Rovamo, 1979; Watson, 1987) and amblyopia (Hess & Howell, 1977; Levi & Harwerth, 1977; Bradley & Freeman, 1981). Importantly for our question, the orientation/detection threshold ratio (Figs. 2E and 3E and averaged across observers and conditions Fig. 3F), is approximately the same in foveal, peripheral and amblyopic vision. This result is somewhat surprising, because we anticipated that increased uncalibrated topographical jitter in peripheral and amblyopic vision would have affected orientation identification to a greater extent than detection.

In order to test the effect of jitter on detection and orientation discrimination directly, we measured thresholds for detection and identification in the presence of stimulus jitter (Section 2). Fig. 4A and B summarize the main results by plotting the orientation/detection threshold ratio (o/d ratio) as a function of the amount of annular jitter for a fixed pattern size (A), and as a function of carrier spatial frequency for several values of jitter specified as a fixed fraction of the center-center patch separation (B). Evidently pattern orientation perception is quite robust to jitter. Jitter of 5′ (Fig. 4A, top ordinate), or 0.3 times the center-center separation (Fig. 4A, bottom ordinate) has only a small effect on the o/d ratio; however, increasing the jitter to 8′, or 0.45 times the center-center separation has a dramatic effect on identification, resulting in an o/d ratio ≈ 4. Fig. 4B shows that jitter of ≈ 0.45 times the center-center separation has a similar effect at 2.5 and 10 c/deg. Note that because we varied spatial frequency by varying the viewing distance, the angular separations and angular jitter differ by a factor of four at these two spatial frequencies, but have the same effect on the o/d ratio. Note that we could have specified the amount of jitter as a fraction of the Gaussian envelope standard deviation (jitter of 0.45 sep is equivalent to 1.35σ), however, we will show below that separation, not σ, determines the tolerance to jitter.

Note that when the jitter is large, the error bars are also large. Inspection of sample psychometric functions (Fig. 4C) shows why. For small amounts of jitter, the psychometric functions for orientation identification are steep (the Weibull slope parameter, beta typically be-

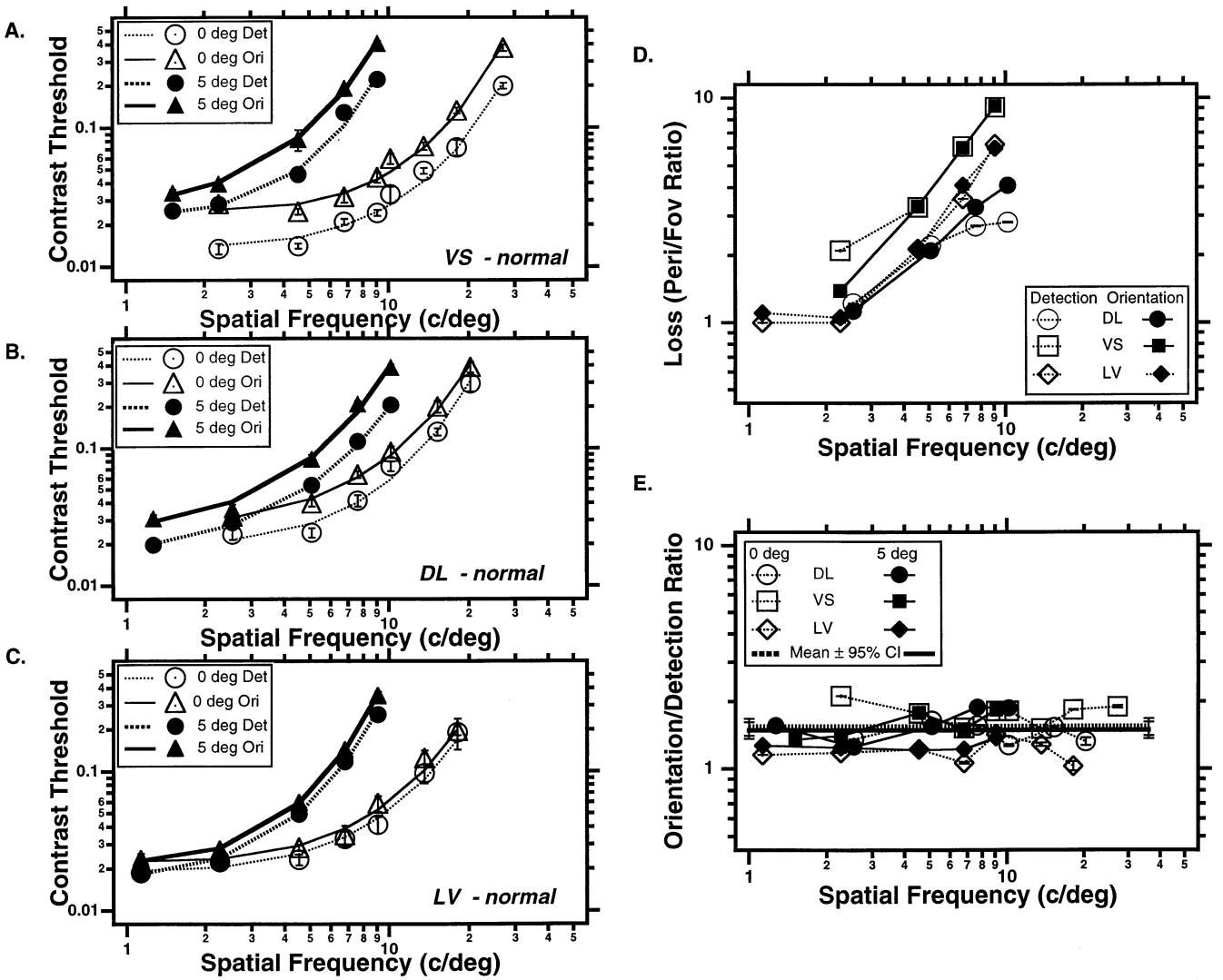

Fig. 2. Panels A-C show contrast thresholds for detection (circles) and orientation identification (triangles) in foveal (open symbols) and peripheral (5° lower visual field-solid symbols) vision as a function of the sample carrier spatial frequency for three normal observers. Panel D shows the loss of contrast sensitivity in peripheral vision (ratio of peripheral/foveal thresholds). Panel E shows the orientation/detection threshold ratio is approximately the same in foveal and peripheral vision.

tween three and four); however, when the jitter is large, performance becomes almost independent of contrast. In the single run sample shown (diamonds), beta was ≈ 0.6 because of a reduced upper asymptote. Thus, flat psychometric functions should be diagnostic of high degrees of jitter. A comparison of the psychometric function slopes (Weibull beta) showed no significant differences between normal fovea and periphery (normal fovea mean 3.92 ± 0.35 (95% confidence interval); periphery mean 4.01 ± 0.42) or between amblyopic and non-amblyopic eyes (mean NAE slope $\approx 2.95 \pm 0.29$; mean AE slope $\approx 2.75 \pm 0.28$), over the range of conditions tested. Thus, we conclude that there must not have been internal jitter in the amblyopic or peripheral visual system greater than about 0.5 times the patch separation.

The results of our simulations with jitter in normal observers also point to a limitation of our method. When the jitter is extreme, performance becomes nearly independent of contrast—thus a more direct approach is to hold contrast fixed and vary the amount of jitter in order to estimate jitter tolerance thresholds directly. This we did in Experiment 2.

3.2. Experiment 2: Jitter thresholds for identification of a suprathreshold E-pattern

This experiment explored the observer's tolerance to positional jitter by measuring 'jitter thresholds' for E-patterns of fixed suprathreshold contrast levels. The main result, illustrated in Figs. 5–7, is that the normal fovea, periphery, and the central field of strabismic amblyopes, all show high tolerance to jitter, with jitter

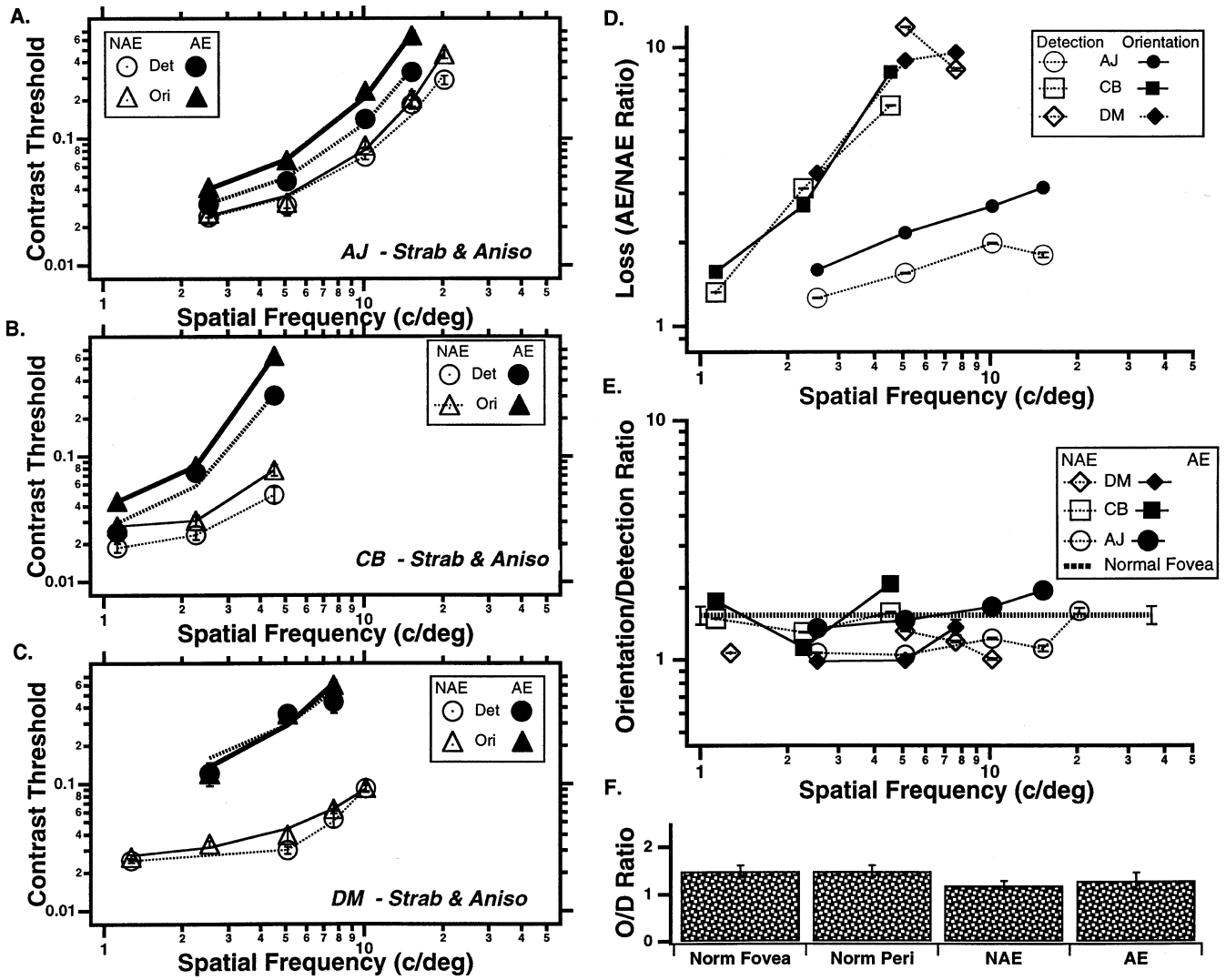

Fig. 3. Panels A-C show contrast thresholds for both detection (circles) and orientation identification (triangles) as a function of the carrier spatial frequency for the nonamblyopic (open symbols) and amblyopic (solid symbols) eyes of three strabismic amblyopes. Panel D shows the loss of contrast sensitivity in amblyopia (ratio of amblyopic/nonamblyopic eye thresholds). Panel E shows the orientation/detection threshold ratio is approximately the same in the nonamblyopic and amblyopic eyes. Panel F shows the orientation/detection threshold ratio averaged across observers and conditions. The ratio is similar in foveal, peripheral and amblyopic vision.

thresholds equal to about half the separation between the patches in each of these visual systems. In Fig. 5A (normal observers) and Fig. 6A (amblyopic observers), the observers' viewing distance was varied. This has the effect of changing the angular size (or standard deviation) of each individual patch, the spatial period of the carrier grating, the separation between the features, and the overall size of the pattern in inverse proportion to the distance. Control experiments show that the jitter threshold is determined by the separation between the features. For example, changing the separation between features, while fixing both the size and period of the features, results in proportional changes in the jitter threshold (Fig. 5B [normals] and Fig. 6B [amblyopic]). Note that patches with different feature sizes (σ in Fig. 5B) with the same separation have nearly identical thresholds. The dotted line in each of these figures shows jitter threshold proportional to ≈ 0.5 times the patch separation. Elsewhere (Levi, Sharma & Klein 1997) we showed that in normal vision, fixing the separation while varying either the spatial period or the standard deviation of the Gabor patches has no effect on the jitter threshold. Thus, tolerance to positional jitter is determined mainly by feature separation, both in normal and amblyopic vision.

The jitter threshold is extremely robust. For example, over a wide range of contrast levels, it is independent of contrast in both normal and amblyopic vision (Fig. 7), and we have shown elsewhere (Levi et al., 1997) that the jitter threshold is independent of the carrier orienta-

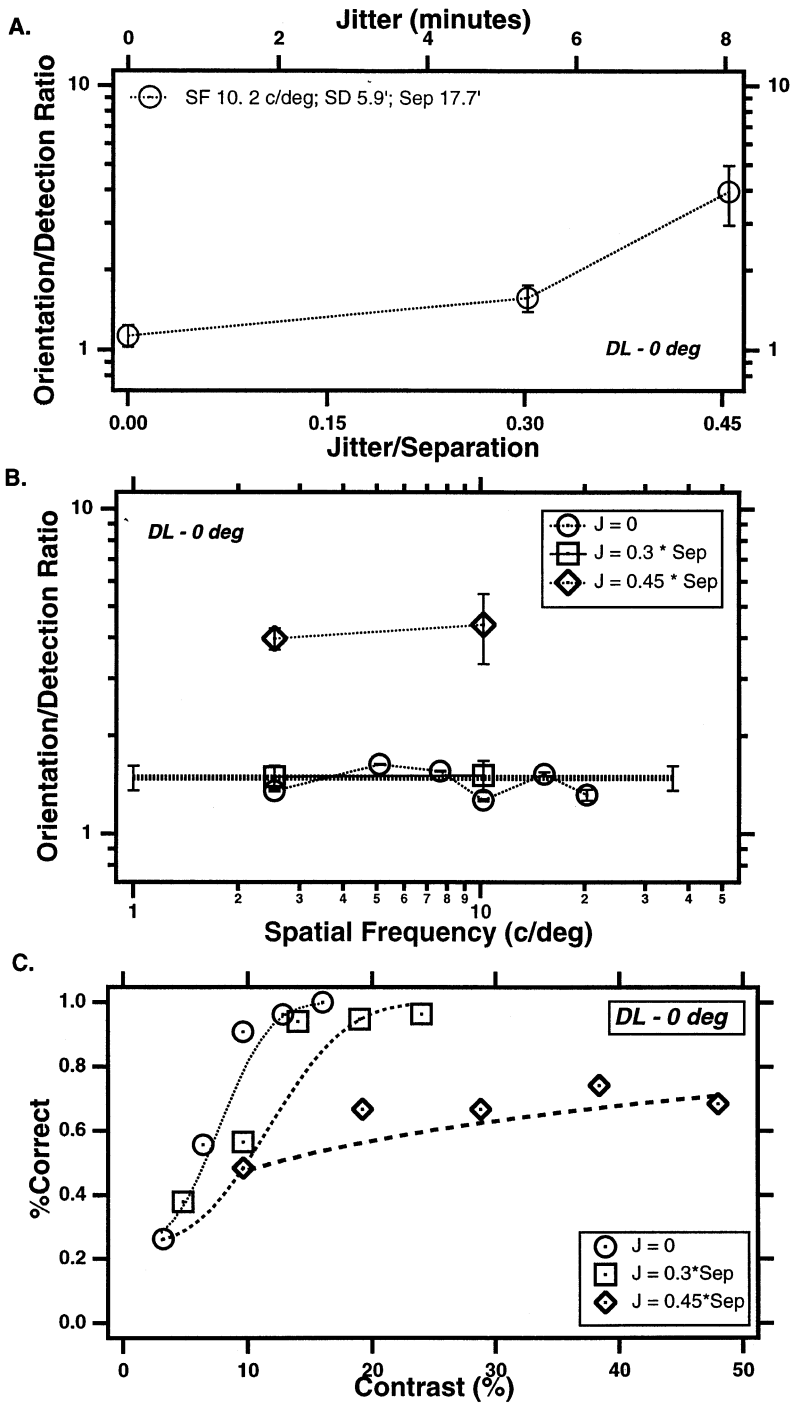

Fig. 4. (A) Shows the orientation/detection threshold ratio (o/d ratio) as a function of the amount of jitter (for a fixed pattern size). The top abscissa shows the jitter specified in minutes of arc. The lower abscissa, shows the jitter specified as a fraction of the center-to-center patch separation. (B) The o/d ratio plotted as a function of carrier spatial frequency for several values of jitter (specified as a fraction of the center-center patch separation). Jitter of 0.45 times the center-center separation has a similar effect at 2.5 and 10 c/deg. Because we varied spatial frequency by varying the viewing distance, the angular separations and angular jitter differ by a factor of four at these two spatial frequencies, but have the same effect on the o/d ratio. (C) Shows samples of the psychometric functions for orientation identification obtained with different amounts of jitter. For small amounts of jitter, the psychometric functions for orientation identification are steep; however, when the jitter is large, the psychometric functions become quite flat as expected from the models in the Appendix.

tion (horizontal, vertical or mixed orientations) and for Gaussian patches, the jitter threshold is also independent of polarity (dark patches, bright patches or mixed polarities). This independence is surprising because detection thresholds for similar targets are about a factor of two worse when the patches have mixed (i.e. both

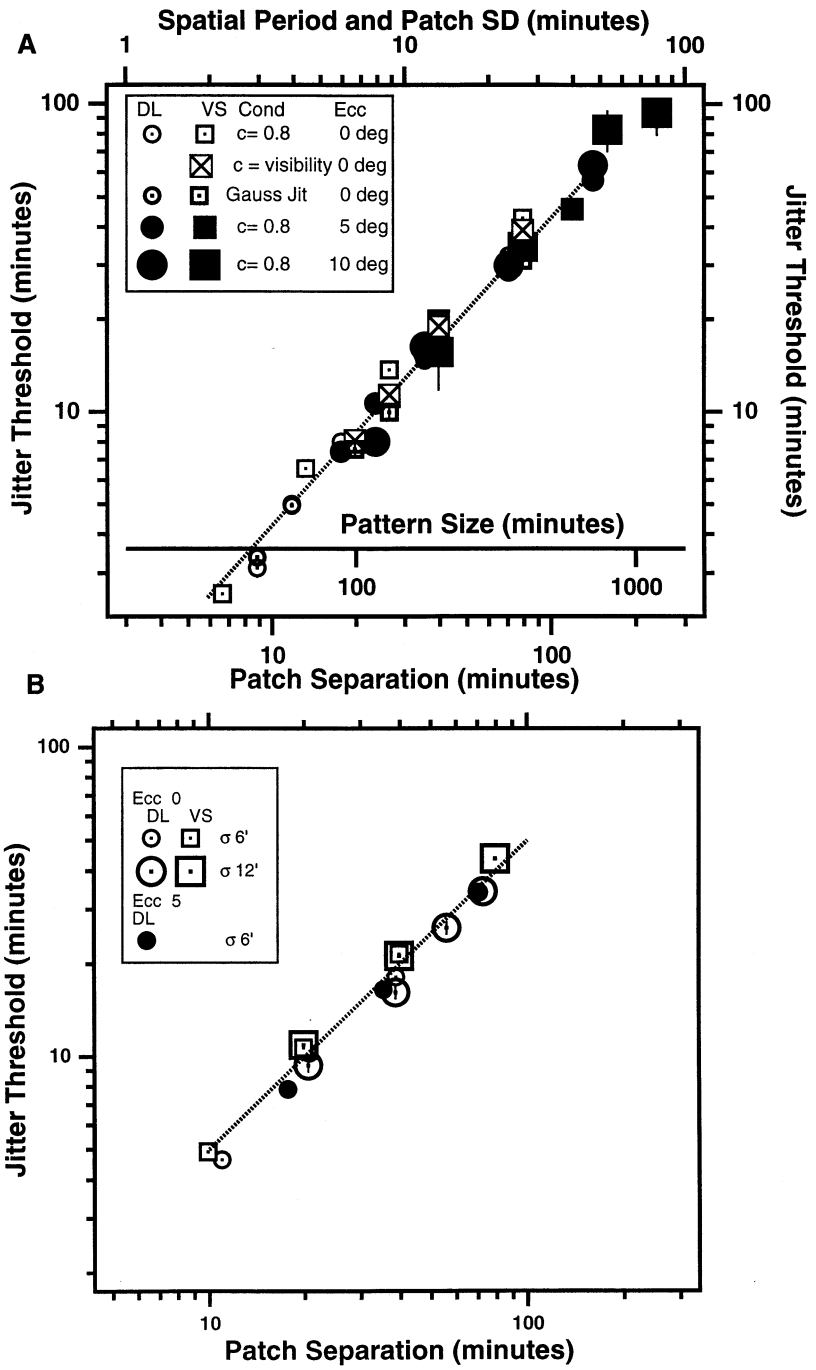

Fig. 5. (A) Jitter thresholds of two normal observers in central (open) and peripheral (5 and 10° in the lower visual field-solid symbols, coded by size). Data shown in this figure were obtained by varying the observers' viewing distance. This has the effect of changing the angular size (or standard deviation) of each individual patch, the spatial period of the carrier grating (standard deviation and spatial period are shown by the upper abscissa), the separation between the features (bottom abscissa), and the overall size of the pattern (internal abscissa), in inverse proportion to the distance. The gray symbols are data using Gaussian jitter, all other data were annular jitter (see Section 2). Squares with X's are foveal data at contrast levels which matched the visibility of the peripheral (5°) stimuli; all other data were obtained with a fixed contrast of 80%. The dotted line shows jitter threshold proportional to ≈ 0.5 times the patch separation. (B) Changing the separation between features, while fixing both the size and period of the features, results in proportional changes in the jitter threshold. Note that patches with different standard deviations (σ's) with the same separation have nearly identical thresholds. Open symbols are foveal data; solid symbols are at 5° in the lower field. The dotted line shows jitter threshold proportional to ≈ 0.5 times the patch separation.

horizontal and vertical) orientations (Saarinen, Levi & Shen, 1997), and spatial interactions at detection threshold are strongest when the elements are aligned.

The high degree of tolerance to jitter makes normal pattern vision quite robust. Interestingly, the same degree of tolerance is evident in normal peripheral vision

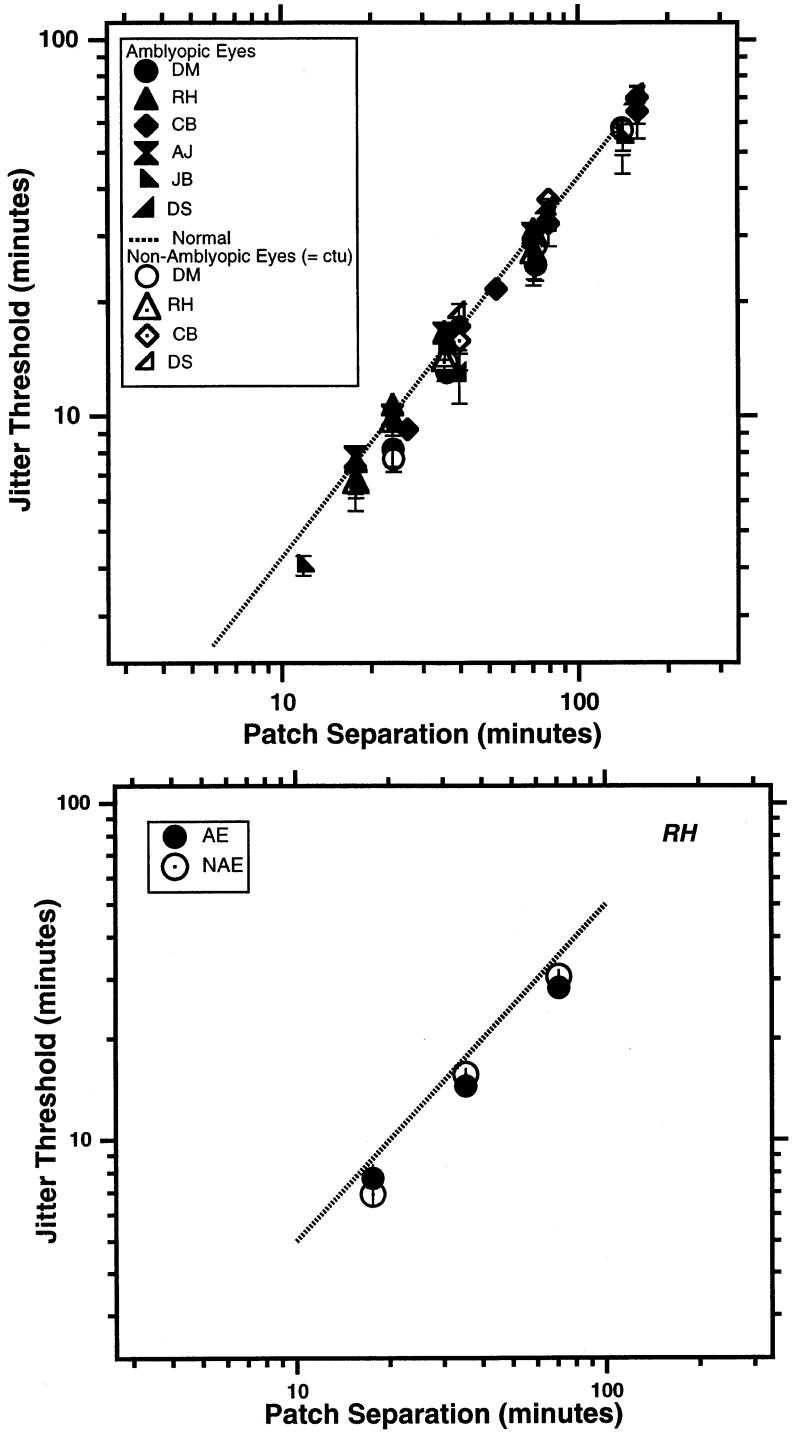

Fig. 6. (A) Jitter thresholds versus separation (obtained by varying the viewing distance as in Fig. 5A), for the amblyopic eyes (solid symbols) of six strabismic amblyopes. The open symbols show data of the nonamblyopic eyes of four of these observers, with contrast levels adjusted to match the visibility of the stimuli in the amblyopic eyes. The dotted line shows jitter threshold proportional to ≈ 0.5 times the patch separation. (B) Changing the separation between features, while fixing both the size and period of the features (similar to Fig. 5B) for each eye of an amblyope, results in proportional changes in the jitter threshold. Note the close similarity of jitter thresholds in the two eyes. The dotted line shows jitter threshold proportional to 0.5 times the patch separation.

and in the central field of humans with naturally occurring strabismic amblyopia. Both the normal periphery and strabismic amblyopes have degraded spatial vision, and one explanation for the degradation is that these visual systems suffer from uncalibrated topographical jitter of cortical receptive fields (Levi & Klein, 1985;

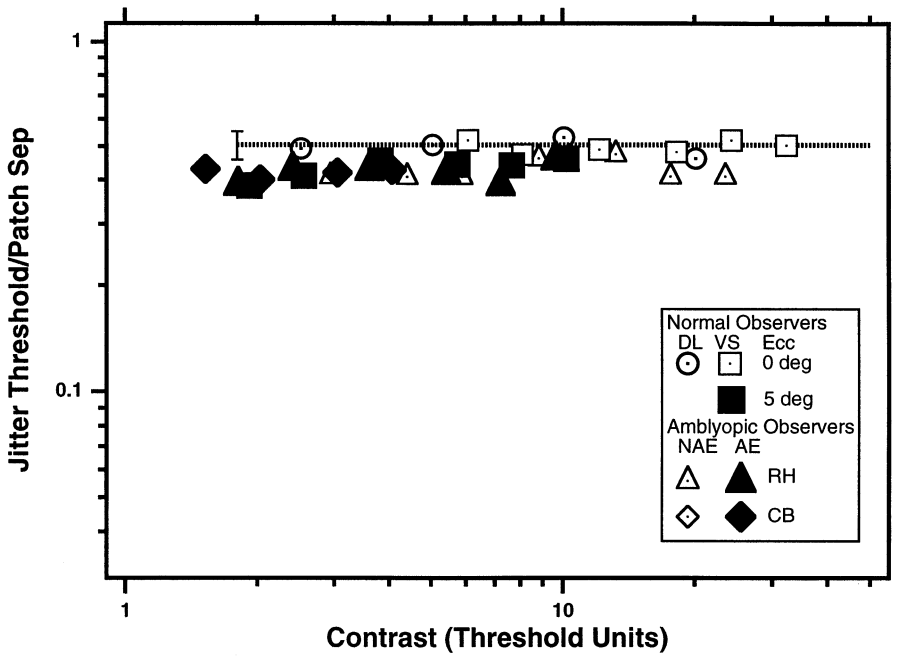

Fig. 7. The jitter threshold is extremely robust to contrast. Over a wide range of contrast levels, from near threshold, it is independent of contrast in the normal foveal (open circles and squares), peripheral (solid squares) and amblyopic (triangles and diamonds) vision.

Levi, Klein & Aitsebaomo, 1985; Hess & Watt, 1990; Wilson, 1991; Hess & Field, 1994; Field & Hess, 1996). Indeed, it has been argued that the topographical jitter can be quite extreme, to the extent of cross-overs in wiring (Hess & Field, 1993, 1994; Hess & McCarthy, 1994). If, in strabismic amblyopia or peripheral vision, the uncalibrated topographical jitter exceeded approximately half the patch separation, then, performance should be degraded (even for unjittered targets, assuming that internal and external jitter have similar effects). However, over the range tested, performance was close to 100% correct for unjittered targets. It should be noted that observers were tested over a large range of pattern sizes; however, the smallest size tested was determined by the visibility of the patterns. In amblyopic and peripheral vision, substantially higher contrast is required to detect small (high spatial frequency) patterns (see Fig. 2 and Fig. 3); for example, at the smallest pattern sizes tested, several of the amblyopes, and the normal periphery showed more than a tenfold loss of contrast sensitivity. Nevertheless, the close similarity in jitter thresholds in foveal, peripheral and amblyopic vision suggests that the computations involved in pattern discrimination are similar in these three visual systems.

We do not wish to imply that there is no increase in uncalibrated topographical disorder in peripheral and amblyopic vision, only that it cannot be so extreme as to limit form perception as defined by our task. Our 'jitter thresholds' might be thought of as providing an upper limit for the jitter which is compatible with form perception (J_{max}). This upper limit is equal to about 0.5 times the separation of the features. In a subset of our observers, we have also measured the smallest amount of jitter that can be detected (J_{min}). Specifically, in a 2-AFC experiment, we showed observers a horizontal string of five Gabor patches (with vertical carriers). One interval contained equally spaced and aligned patches, and the other contained the same five patches subjected to two-dimensional Gaussian jitter. The observer's task was to decide which interval contained the jitter (experimental details and detailed results will be given in a separate publication). As can be seen in Fig. 8, J_{min} for the normal fovea is more than 20 times smaller than J_{max} (about 0.02 [$^1/_{50}$] of the patch separation over most of the range of separations for which we also measured J_{max}). At the largest separations, J_{min} is similar in normal fovea, periphery and amblyopia; however, at smaller separations, J_{min} levels off at about 3′ in the periphery (5°, lower visual field), and compatible with $E_2 \approx 0.8$ degs, and at about 2′ in the central field of this particular strabismic amblyope. While we have not directly estimated the intrinsic jitter of these observers, we believe that the elevated J_{min} values are closely related to the increase in topographic jitter (Levi & Klein, 1985; Hess & Watt, 1990; Wilson, 1991; Hess & Field, 1993, 1994; Hess, McIlhagga & Field, 1997). More importantly, given the high degree of tolerance of form discrimination to jitter, J_{max} would not be affected by the elevated intrinsic jitter until the separation between elements were on the order of 4–6 min (twice the

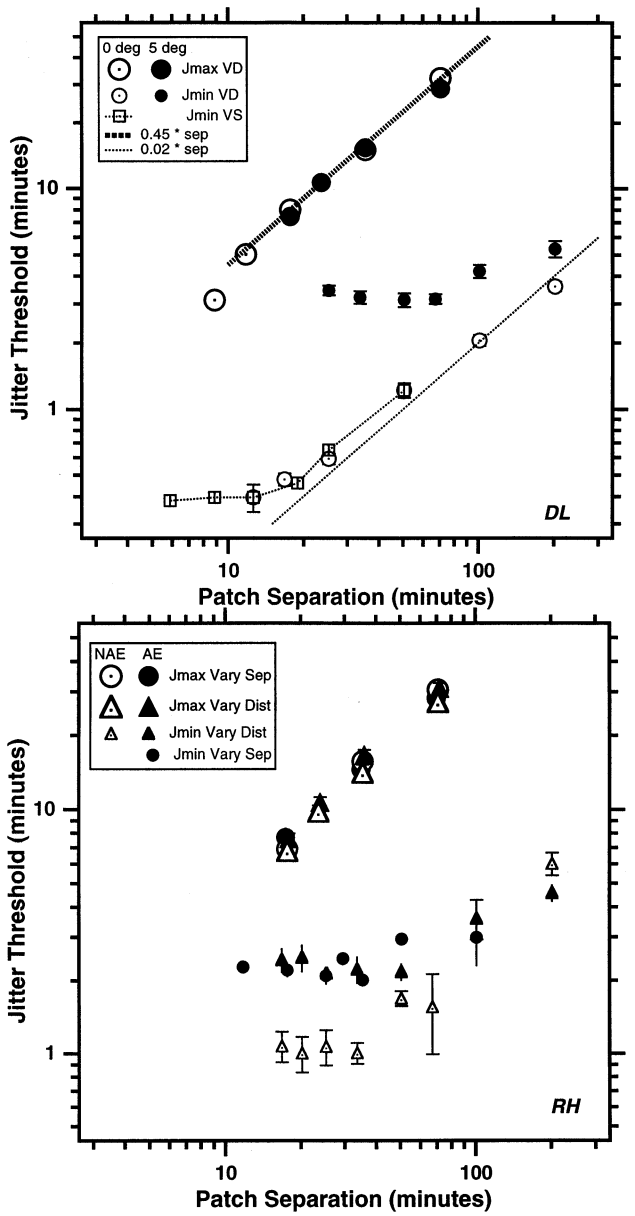

Fig. 8. (A) Replots the jitter thresholds for observer DL at 0° (open large circles) and 5° (solid large circles) in the lower visual field. The thick dotted line shows threshold $= 0.45*$ separation. These jitter thresholds provide an upper limit for the jitter which is compatible with form perception (J_{max}). The small symbols show the smallest amount of jitter that can be detected (J_{min}) in a string of five Gabor patches (similar to one side of our E). J_{min} was determined either by varying the viewing distance (small circles—which resulted in variation of the separation, patch size (S.D.) and spatial frequency) or by fixing the distance (patch size and spatial frequency) and varying the separation on the display (squares). For the normal fovea J_{min} is more 20 times smaller than J_{max} (about 0.02* separation-thin dotted line) over much of the range of separations for which we also measured J_{max}. At the largest separations, J_{min} is similar in normal fovea, and periphery; however, at smaller separations, J_{min} levels off at about 3′ in the periphery (5°, lower visual field). (B) Similar to Fig. 8A, but for each eye of strabismic amblyope RH. Note that for this observer, J_{min} is similar in the two eyes at large separations; however, at small separations it levels out at about 2′ in the amblyopic eye-about a factor of two higher than the fellow eye. We believe that the elevated levels of J_{min} in both the amblyopic eye and in the periphery reflect elevated levels of intrinsic jitter.

intrinsic jitter). However, at these close separations the associated high spatial frequencies make the stimuli practically invisible to both the amblyopic eye and the peripheral visual field.

3.3. Experiment 3: Sample thresholds for identification of a suprathreshold E-pattern

How many stimulus features (samples) are required for pattern identification in peripheral and amblyopic vision? In this experiment we determined what fraction of the 17 Gabor samples are needed to reliably identify the orientation of the E-patterns by measuring a 62.5% correct 'sample threshold'. In foveal vision, over a broad range of stimulus conditions, the 'sample' threshold is ≈ 40–50% of the 17 total samples comprising our E-pattern, and the sample threshold is independent of patch standard deviation, separation, carrier spatial period and patch details (Levi et al., 1997). The new result, shown in Fig. 9B, is that strabismic amblyopes, like the normal periphery (Fig. 9A) require more samples than the normal fovea, even when the pattern visibility is matched. The difference between the normal fovea, and peripheral and amblyopic vision is largest at high spatial frequencies (small patches). For the smallest sizes at which the observers could perform the task (i.e. the contrast of the pattern was at least twice the contrast threshold for orientation discrimination), the sample threshold of the periphery and strabismic amblyopes was about 70%—an increase of about 55% relative to the normal fovea (Fig. 9). This increase in the sample threshold is not simply a visibility effect. As reported previously, in the normal fovea, the sample threshold is almost independent of contrast (Levi et al., 1997) (see Fig. 10, open symbols). It is also largely independent (unpublished observations) of stimulus duration (55 ms–2 s) and mean luminance (over a 2 log unit range). Fig. 10 (solid symbols) shows that the sample threshold is also elevated over a range of target contrasts, in amblyopic and peripheral vision. Note that the highest contrast levels correspond to a physical (stimulus) contrast of 100%. The increased 'sample' threshold in peripheral vision and strabismic amblyopia (even after scaling the target visibility) suggests that in these visual systems, the stimulus is underrepresented at the stage of feature integration, perhaps due to undersampling (Levi & Klein, 1986; Levi et al., 1987; Wilson, 1991; Levi et al., 1994a; Levi et al., 1994b; Levi & Klein, 1996).

4. Modeling the effects of undersampling and jitter on Form discrimination

Ideal-observer models provide a useful means for understanding human performance. Specifically, ideal

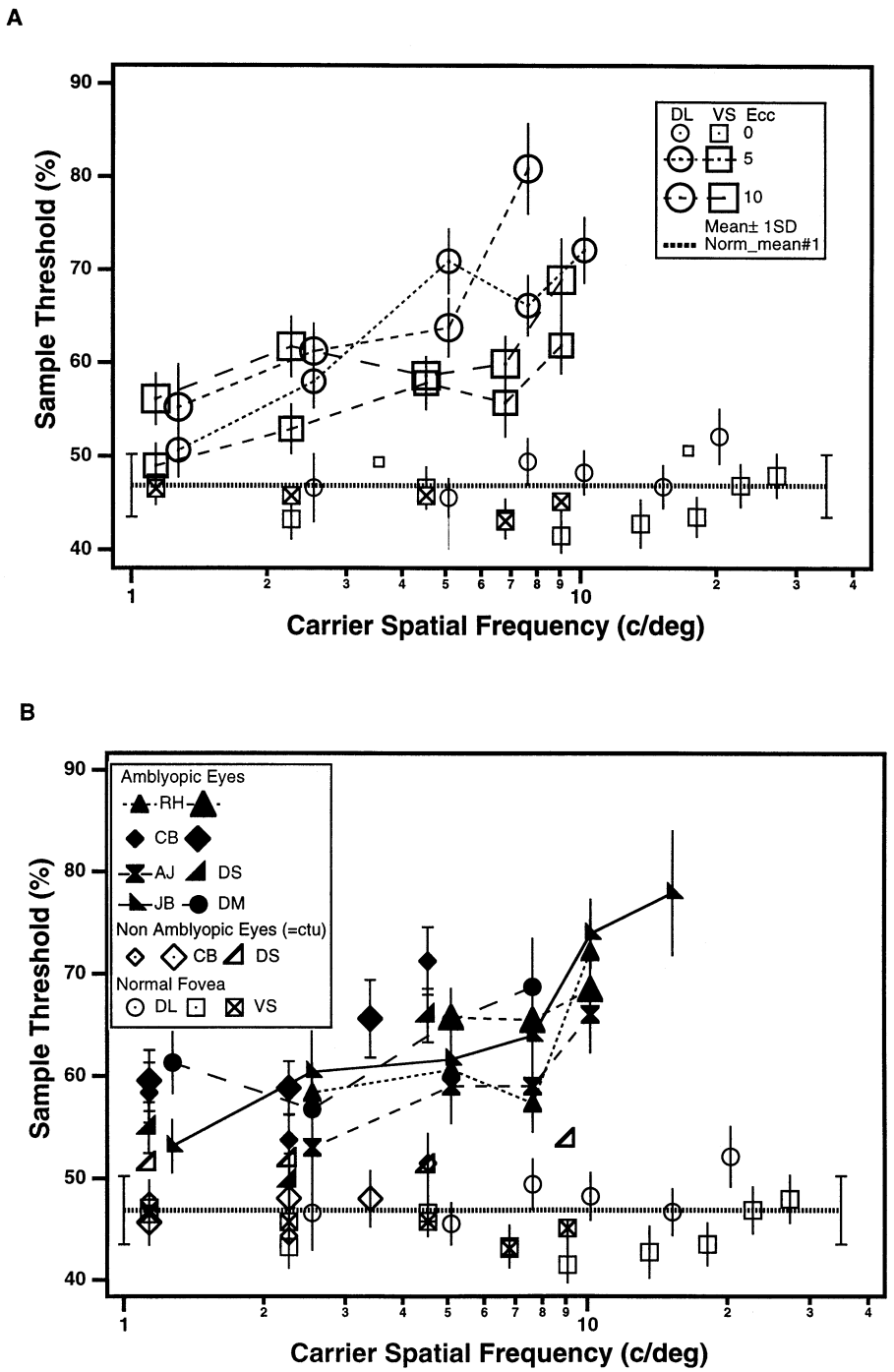

Fig. 9. (A) Sample threshold for two normal observers viewing foveally (small symbols) or at 5° and 10° in the lower visual field (large symbols). Open circles and squares were obtained with high contrast (80%) features by varying the viewing distance and are plotted as a function of the carrier spatial frequency. The horizontal dotted line shows the mean (± 1 S.D.) threshold of the normal fovea is about 45% of the sample. Squares with crosses are foveal data obtained with the feature contrast adjusted to match the visibility at 5° in the periphery. (B) The data of the normal fovea from Fig. 9A are replotted here along the data of the amblyopic eyes of six strabismic amblyopes (solid symbols). Note that like the periphery (large symbols in Fig. 9A), the sample thresholds of the amblyopic eyes are elevated, especially at high spatial frequencies. Also shown are the fellow eyes of three amblyopes, with the feature contrast adjusted to match the visibility with the amblyopic eye.

observer models enable one to determine how much information was lost (or transmitted) by the visual system, to compare human performance in different tasks, and, most importantly for our study, to provide a metric for understanding the information in the stimulus (Geisler, 1989). Therefore we have applied ideal-observer modeling to our E-like stimuli and discrimination tasks. Ideal-observer modeling has previ-

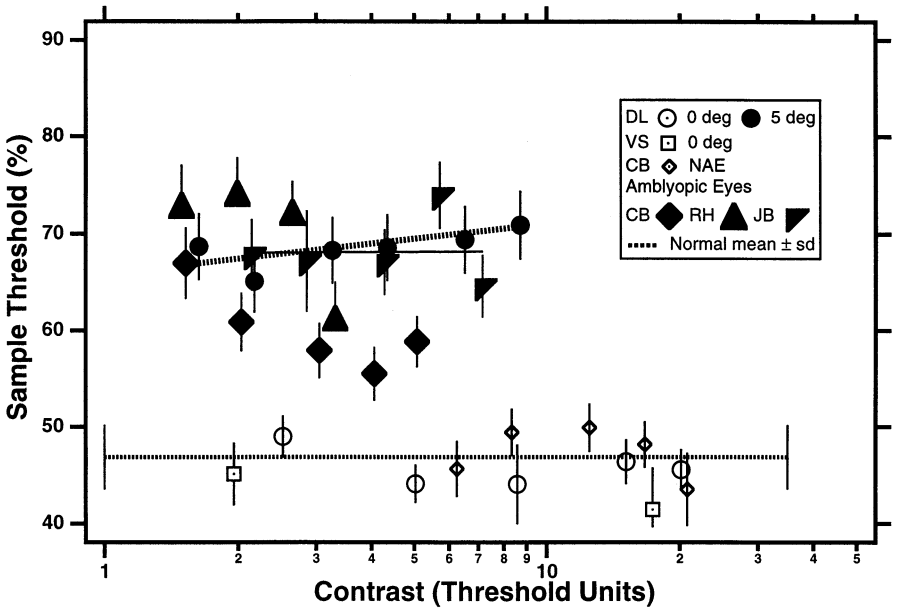

Fig. 10. In the normal fovea (open symbols) sample thresholds are nearly independent of stimulus contrast (specified in threshold units). In peripheral (solid circles) and amblyopic (solid diamonds and triangles) vision the sample threshold is elevated over a range of target contrasts. Note that the highest contrast levels correspond to a physical (stimulus) contrast of 100%.

ously been used in letter identification tasks (Parish & Sperling, 1991; Solomon & Pelli, 1994).

4.1. Undersampling—human and ideal performance compared

Elsewhere (Levi et al., 1997) we showed that an ideal observer based on the joint probabilities of losing critical sample pairs, is slightly better of humans using their fovea. The ideal sample threshold was $\approx 31\%$ (i.e. 31% of the samples were sufficient to achieve 62.5% correct performance), compared to optimal human performance of about 40–50%. Thus the normal fovea is quite efficient in using the samples, whereas peripheral and strabismic amblyopic vision are rather inefficient. In the Appendix (A.1.) we describe this model in detail, and discuss some of its predictions. In this section we compare the model predictions to human performance. While the 'sample thresholds' reported above are based on the overall error rate, both ideal and human observers make different kinds of errors when judging the orientation of an E-like pattern. Specifically, one can categorize the type of error as being either a 180° error, in which the observer's report is the mirror image of the actual orientation (e.g. the observer confuses up for down or left for right) or a 90° error in which the observer confuses, e.g. up or down with left. Fig. 11 (top) illustrates the four stimulus orientations, and the types of response error. The ideal observer model predicts different error rates for 180° errors than for 90° errors.

Fig. 11A shows the ideal observer's performance plotted as a function of the probability of losing a sample. The thick solid line shows the probability of making no errors of any type (p correct). As expected, the probability of making no errors decreases as the probability of losing samples increases. The dotted and dashed lines show the probability of making 180° and 90° errors, respectively. Note that for low abscissa values, the ideal observer makes more 180° (mirror) errors than 90° errors; however, when the probability of losing a sample is high (i.e. a sparsely sampled E), the ideal observer makes more 90° errors.

Fig. 11B shows that human observers perform qualitatively similarly to the ideal observer. Shown here are the psychometric functions of all of the foveal data of observer DL contributing to Fig. 9A averaged across the eightfold range of spatial frequencies (viewing distances). Each datum is based on ≈ 600 trials. The close similarity between the human and ideal observer is clearly evident. The curves are the ideal observer predictions, shifted along the horizontal axis by multiplying the ideal X-axis values by 0.85, i.e. the human performs with an efficiency of $\approx 85\%$. Like the ideal observer, the human observer also shows a crossover, with 90° errors dominating when the probability of losing a sample is high, and 180° errors being somewhat larger at low probabilities. At the highest probability of losing a sample (0.8 on the abscissa), the human observer guesses, and the probabilities of making 90 and 180° errors approach 50 and 25%, respectively (as do the model probabilities).

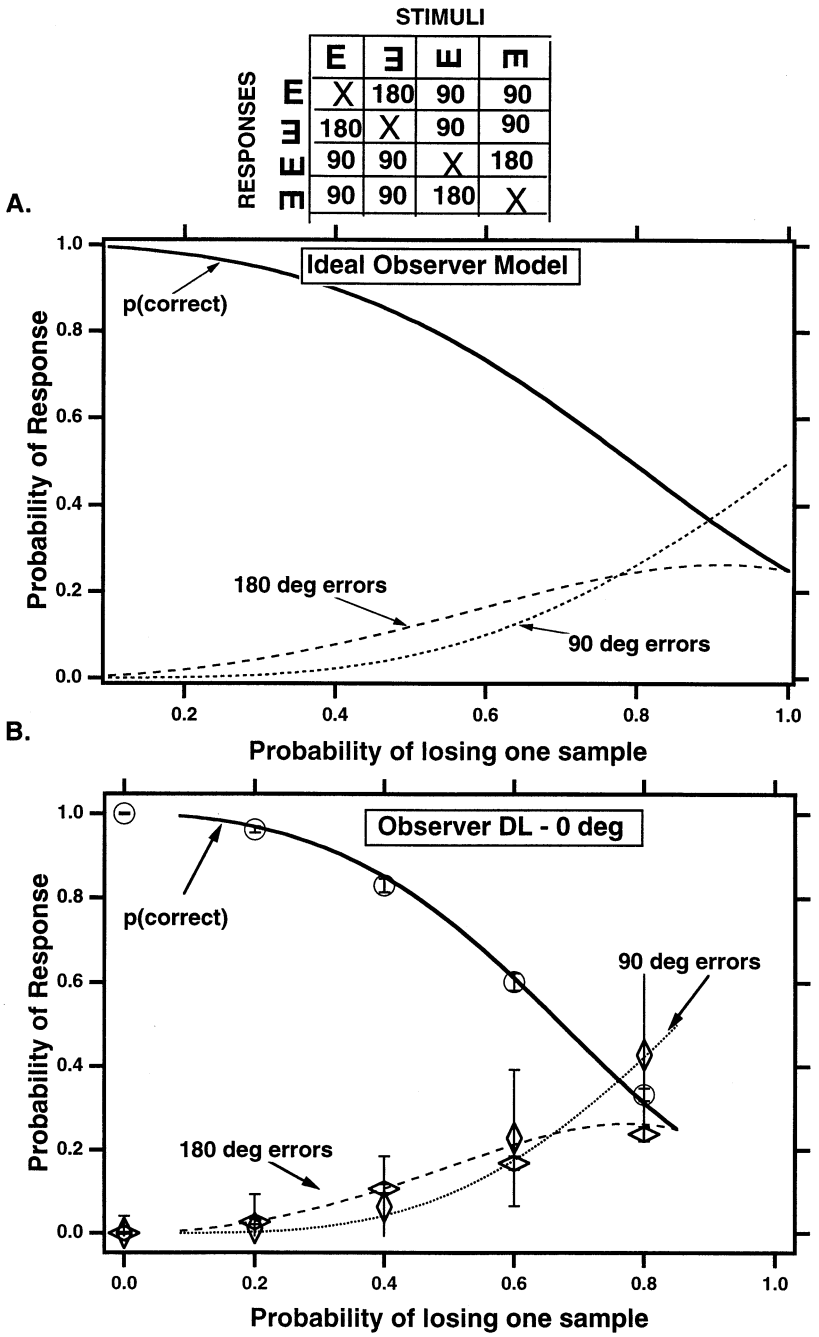

RESPONSES \ STIMULI	E	3	Ш	m
E	X	180	90	90
3	180	X	90	90
Ш	90	90	X	180
m	90	90	180	X

Fig. 11. The inset in Fig. 11 illustrates the four stimulus orientations, and the types of response error. (A) The ideal observer's performance plotted as a function of the probability of losing a sample. The thick solid line shows the probability of correct responses (i.e. making no errors of any type). The dotted and dashed lines show the probability of making 180° and 90° errors, respectively. (B) The symbols show the psychometric functions of all of the foveal data of observer DL from Fig. 9A, averaged across the eightfold range of stimulus sizes. Each datum is based on ≈ 600 trials, and each of the three probabilities (p (correct), i.e. no errors (circles), 90° errors (tall diamonds) and 180° errors (wide diamonds)) are shown. The lines are the ideal observer predictions (from Fig. 11 A), shifted along the horizontal axis by multiplying the ideal X-axis values by 0.85 (i.e. an efficiency factor of 0.85).

4.2. Jitter—human and ideal performance compared

The Appendix (A.2.) considers three classes of models for predicting the results for the case when the sample locations were jittered by Gaussian noise: (1) an ideal observer model, maximum likelihood without replacement; (2) a template model similar to the ideal observer model, maximum likelihood with replacement; and (3) a model based on the asymmetry of the samples in the horizontal and vertical directions. As discussed in the Appendix (A.2.), the ideal observer model (1) for jitter is impractical (requiring calculation of the likeli-

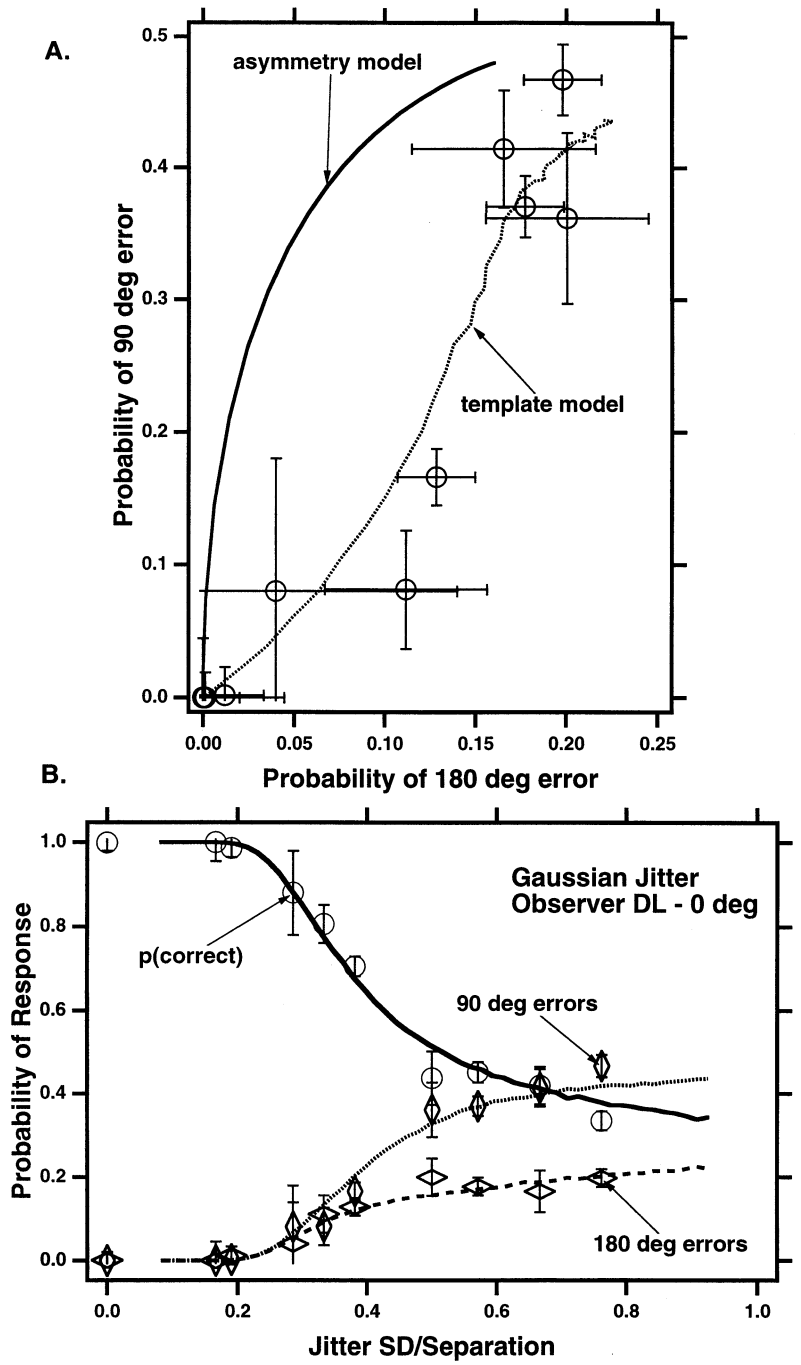

Fig. 12. (A) Plots the probability of making a 90° versus 180° error in the jitter task. The data (circles) are the psychometric functions from all of the foveal Gaussian jitter data of observer DL in Fig. 5A, averaged across an eightfold range of viewing distances. The lines show the predictions of two models of jitter: the signal detection asymmetry model (solid line) and the template model (dotted line). The model details are provided in the Appendix A(A.2.). The data fall close to the predictions of the template model. (B) Plots the response probabilities (as in Fig. 11) as a function of the magnitude of the jitter, specified as a fraction of the sample separation (jitter/separation) for both the human observer (circles and diamonds) and the template model (the lines are the template model predictions, shifted along the horizontal axis by multiplying the template model X-axis values by an efficiency of 0.66).

hood of the 17! possible correspondences between the jittered data and the four templates). In this section we compare human performance to the predictions of both the asymmetry (3) and the template model (2).

In order to make a direct comparison between our data and the two models, Fig. 12A compares the asymmetry and template model predictions by plotting the probability of a 180° error against the probability of a 90° error (see Appendix (A.2) for calculation). This plot is useful in that it is independent of the magnitude

of jitter. Only the type of error is relevant. Note that in this figure the asymmetry model predicts much greater 90° than 180° errors. The data shown are from the psychometric functions from all of the foveal Gaussian jitter data of observer DL from Fig. 5A, averaged across an eightfold range of viewing distances (each datum is based on ≈ 700 trials). Note that the data fall close to the predictions of the template model, but far from the predictions of the asymmetry model—so we can reject this class of models. Moreover, the asymmetry model performs worse than our human observers, providing additional grounds for rejection.

The close match between the predictions of the template model and human performance can be seen more closely in Fig. 12B, which plots the response probabilities (as in Fig. 11) as a function of the magnitude of the jitter, specified as a fraction of the sample separation (jitter/separation) for both the human observer (circles) and the template model (the lines are the template model predictions, shifted along the horizontal axis by multiplying the template model X-axis values by an efficiency of 0.66). Like the model, the human observer also shows 90° errors dominating when the probability of losing a sample is high. However, it is interesting to note that the human observer is more efficient relative to the model (85 versus 66%) in the sample task than in the jitter task (if compared to an ideal observer for the jitter task the efficiency would likely be lower than 66%).

5. General discussion

The mechanisms of feature integration appear to operate by assigning 'place tags' to each sample (Levi et al., 1997). The positional tolerance of these place tags is about half of the separation between the features in foveal, peripheral and amblyopic vision; and, in foveal vision, each feature requires only about a 50% probability of being present for reliable discrimination. Our results provide an upper limit of stimulus jitter for accurate form perception in normal vision. Any uncalibrated intrinsic positional jitter in peripheral and amblyopic vision must not exceed this limit. The increased 'sample' threshold in peripheral vision and strabismic amblyopia (even after scaling the target visibility) suggests that in these visual systems, the stimulus is underrepresented at the stage of feature integration, perhaps due to undersampling. Thus, in peripheral and amblyopic vision, removing samples degrades performance because these visual systems need every sample (i.e. they lack the redundancy present in normal foveal vision). Since the samples are visible, we speculate that the increased sample threshold reflects a form of visual 'neglect' in the normal periphery, and in the central field of strabismic amblyopes.

Our study does not imply that strabismic amblyopes, or peripheral vision do not have raised levels of intrinsic positional uncertainty. Indeed, recent studies (Hess et al., 1997; Wang, Levi & Klein, 1998), and the $J_{\min}$ data of the present paper (Fig. 8), are all consistent with an elevated level of internal jitter in these visual systems. On the other hand our results suggest that the internal jitter is not so extreme as to disrupt the perception of simple isolated patterns (Fahle & Bachmann, 1996). A recent study (Hess et al., 1997) measured performance on a task involving the detection of paths composed of micro patterns (Gabor patches) with correlated carrier orientations embedded in a field of similar patches with random position and orientation. Performance of the amblyopic eye was reduced on this task (at a scale factor of two below the acuity limit), and the reduced performance could be mimicked in the normal eye by adding noise, equivalent to the estimated intrinsic noise of the amblyopic eye. Hess and colleagues suggest that the rules by which cellular outputs are combined in their task are normal, and we agree (Levi & Sharma, 1998); however, while Hess et al. show that intrinsic positional uncertainty is a sufficient explanation for the reduced performance of the amblyopic eye, this does not preclude alternative explanations such as reduced sampling efficiency (Wang et al., 1998) at high spatial frequencies. Hess and Anderson (1993) argue against undersampling, because they were not able to demonstrate motion reversal in their amblyopic subjects using directly viewed gratings. The failure to observe motion reversal does not necessarily imply that undersampling does not occur (Artal, Derrington & Colombo, 1995; Wang, Thibos & Bradley, 1996). Recent experiments, using coherent light, have demonstrated large errors in perceived orientation in the central field of strabismic amblyopes (including two of the observers in our study) at spatial frequencies much lower than the cone Nyquist limit. The inability to make veridical orientation matches is consistent with undersampling at a post-receptoral stage (Sharma, Levi & Coletta, 1997), as is the marked loss in sampling efficiency in strabismic amblyopes recently reported by Wang et al. (1998). While there is a great deal of redundancy in the cortical representation of the normal fovea (due to the large divergence between optic tract fibers and V1 neurones), the dramatic loss of cortical neurons driven through the amblyopic eye (Baker, Grigg & von Noorden, 1974; Wiesel, 1982) could provide a neural substrate for undersampling, and the sampling issues (statistical, not visual) involved in looking at cell losses may actually underes-

timate the losses (since one cannot count cells that do not respond). Moreover, the 'undersampling' may occur at a level beyond V1. For example, a recent functional imaging study (PET) in human amblyopes found a selective reduction of activation in Brodmann areas 18 and 19 when the visibility of the patterns was equated in the amblyopic and nonamblyopic eyes (Imamura, Richter & Fischer, 1997).

Our experiments and modeling suggest that the normal human fovea is highly efficient in using the samples to determine the orientation of our E-like pattern (we were able to match human foveal performance to ideal performance by an efficiency factor of 0.85). At high spatial frequencies, both peripheral and amblyopic visual systems are much less efficient (see Fig. 9). On the other hand, observers (normal fovea, periphery and amblyopic) are not as efficient in unscrambling the positions of jittered samples when all are present (a match between the human and template model required an efficiency factor of 0.66, and efficiency would likely be lower when compared to an ideal observer model). The models described in the Appendix were designed for our simple, isolated patterns, however, this class of models may have relevance for other tasks, such as judgments of curvilinearity (Feldman, 1997) or more complex tasks such as detection of curved paths (Field, Hayes & Hess, 1993).

Acknowledgements

We are grateful to Hope Marcotte-Queener for programming. This research was supported by research grants (RO1 EY01728 and RO1 EY04776), and a Core grant (P30EY07551) from the National Eye Institute, National Institutes of Health, Bethesda MD.

Table 2
Error probabilities

Lines present	No error	90° Error	180° Error	Probability
T M B S	1	0	0	$(1\text{-}p^2)^4$
M B S	1	0	0	$p^2\ (1\text{-}p^2)^3$
T B S	1	0	0	$p^2\ (1\text{-}p^2)^3$
T M S	1	0	0	$p^2\ (1\text{-}p^2)^3$
T M B	1/2	0	1/2	$p^2\ (1\text{-}p^2)^3$
B S	1/2	1/2	0	$(p^2)^2\ (1\text{-}p^2)^2$
M S	1	0	0	$(p^2)^2\ (1\text{-}p^2)^2$
M B	1/2	0	1/2	$(p^2)^2\ (1\text{-}p^2)^2$
T S	1/2	1/2	0	$(p^2)^2\ (1\text{-}p^2)^2$
T B	1/2	0	1/2	$(p^2)^2\ (1\text{-}p^2)^2$
T M	1/2	0	1/2	$(p^2)^2\ (1\text{-}p^2)^2$
S	1/3	2/3	0	$(p^2)^3\ (1\text{-}p^2)$
B	1/3	1/3	1/3	$(p^2)^3\ (1\text{-}p^2)$
M	1/2	0	1/2	$(p^2)^3\ (1\text{-}p^2)$
T	1/3	1/3	1/3	$(p^2)^3\ (1\text{-}p^2)$
None	1/4	1/2	1/4	$(p^2)^4$

Appendix A

A.1. Ideal observer model for sampled E

This section presents an ideal observer model for identifying the orientation of the E target when samples are removed. The E consists of four lines: M (middle), T (top), B (bottom) and S (side—the vertical stroke). Table 2 shows the probability of making three types of error (no error, 90° or 180° error) for different combinations of the presence of the four types of lines.

The left column lists which of the lines are present. For a line to be present either the second and/or the fourth samples in that line must be present. The first, third and fifth samples of any of the four lines are irrelevant since these samples are common to all the orientations and thus they carry no information about orientation. The second column gives the probability of judging the orientation correctly. The third and fourth columns are the probabilities of making 90° and 180° errors. Consider, for example, the fifth row in which the top, middle and bottom lines are present and the side line is missing (TMB in column 1). With the side line missing, two orientations are possible: original and the 180° rotation. Each of these possibilities have equal likelihood so a half is placed in the second and fourth column. Consider now, the reversed case found in the twelfth row where only the side line remains. Now three orientations are equally possible: the original, and the two 90° rotations. Thus there is a 1/3 chance of guessing the correct orientation and a 2/3 chance of making a 90° error. These values are found in columns two and three.

The right column gives the probability of each of the 16 possible line combinations in terms of P, the probability of losing a single sample. The probability of losing a given line is P^2 since both the second and the fourth samples must be missing for the ideal observer to declare that the line is gone. For example, if $P = 1/4$, then the probability of losing both the top and the bottom lines are $(P^2)^2 = 1/256$. The probability of not losing a line is $(1 - P^2)$. Thus the probability of losing two specific lines and not losing the other two is $(P^2)^2\ (1 - P^2)^2$. These are the quantities listed in column 5.

Finally by multiplying columns 2, 3 and 4 by column 5, and then summing down the three columns, we obtain the probability of each of the three judgments. These are the probabilities that are plotted in Fig. 11.

$$\text{prob}_{\text{correct}} = (1 - P^2)^4 + 7/2P^2(1 - P^2)^3 + 7/2(P^2)^2(1 - P^2)^2 + 3/2(P^2)^3(1 - P^2) + 1/4(P^2)^4$$

$$\text{prob}_{90\ \text{error}} = (P^2)^2(1 - P^2)^2 + 4/3(P^2)^3(1 - P^2) + 1/2(P^2)^4$$

$$\text{prob}_{180\ \text{error}} = 1/2\ \ P^2(1 - P^2)^3 + 3/2\ \ (P^2)^2(1 - P^2)^2 + \ \ 7/6(P^2)^3(1 - P^2) + 1/4(P^2)^4$$

Note that the three probabilities add up to unity for any value of P.

For small values of P the leading terms are:

$$\text{prob}_{\text{correct}} = 1 - 1/2\ P^2 + \text{order of } P^4$$

$$\text{prob}_{90\text{ error}} = P^4 + \text{ order of } P^6$$

$$\text{prob}_{180\text{ error}} = 1/2\ P^2 + \text{ order of } P^4$$

This behavior shows that the 180° errors dominate the 90° errors for low values of P. For large values of P (small values of $1 - P^2$) the leading terms are:

$$\text{prob}_{\text{correct}} = 1/4 + 1/6\ (1 - P^2) + \text{ order of } (1 - P^2)^2$$

$$\text{prob}_{90\text{ error}} = 1/2 - 2/3\ (1 - P^2) + \text{ order of } (1 - P^2)^2$$

$$\text{prob}_{180\text{ error}} = 1/4 + 1/2\ (1 - P^2) + \text{ order of } (1 - P^2)^2$$

It is surprising to note that for values of P near unity the 180° errors are a decreasing rather than increasing function of P. This reversed behavior can be seen in Fig. 14B.

A.2. Model predictions for jittered E

This section considers three classes of models for predicting the results for the case when the sample locations were jittered by Gaussian noise: (1) the ideal observer model, maximum likelihood without replacement; (2) a template model similar to the ideal observer model, maximum likelihood with replacement; and (3) a model based on the asymmetry of the samples in the horizontal and vertical directions.

A.2.1. Model 1: Maximum likelihood ideal observer model

The ideal observer would calculate the likelihood that the observed jittered samples had come from each of the four possible E patterns. The steps in the calculations are:

1. Iterate over the four possible E orientations.
2. Iterate over all 17 factorial (17!) possible correspondences, C, of the unjittered and jittered sample locations.
3. For each possible correspondence calculate the likelihood of one of the data samples coming from the corresponding template sample. The x and y components of the jth jittered sample is given by (D_{jx}, D_{jy}), where j ranges from 1 to 17. The x and y components of the ith unjittered sample, for the kth template (k ranges from 1 to 4 corresponding to the four possible orientations) is given by (T_{kix}, T_{kiy}) where i ranges from 1 to 17. The likelihood for the jth data sample to have come from the corresponding sample of the kth template is proportional to:

$$L_K(C, j) = \exp(-((T_{kix} - D_{jx})^2 + (T_{kiy} - D_{jy})^2)/2\sigma^2) \quad (1)$$

where i is a number from 1 to 17 that is fixed, once the correspondence, C, and datum, j, are specified. The Gaussian factor arises from the Gaussian nature of the jitter process, and σ is the standard deviation of the jitter in sample separation units (the quantity on the abscissa in Fig. 4A and Fig. 11).

4. Calculate the total likelihood for that particular correspondence. The total likelihood is the product over all 17 factors in Eq. (1). Maximizing the total likelihood gives the same results as minimizing the negative logarithm of the likelihood function. The total log likelihood for each of the four orientations is given by (up to a constant of proportionality):

$$LL_k(C) = \sum_{j=1}^{17} (T_{kix} - D_{jx})^2 + (T_{kiy} - D_{jy})^2 \quad (2)$$

The summation is a single summation over j since the index i is fixed according to the correspondence. Maximizing the quantity in Eq. (2) is the same as maximizing the summed correlation function which come from the cross terms of the expanded Eq. (2):

$$\text{correlation} = \sum_{j=1}^{17} T_{kix}D_{jx} + T_{kiy}D_{jy} \quad (3)$$

because the sum of the squares of T_{kix} and T_{kiy} in Eq. (2) are a constant, independent of orientation. The same is true for D_{jx} and D_{jy}.

5. Determine which likelihood is maximum across all 17! correspondences and four orientations. Respond by choosing the orientation with that maximum likelihood.

The problem with this method is that there are $17! \approx 3.5569*10^{14}$ possible correspondences for each orientation. This is much too large a number for practical calculations. The following two methods depart from the ideal observer, in favor of a speedier computation.

A.2.2. Model 2: Template model: likelihood with replacement

The second model to be considered is a template model that is similar in spirit to model 1. The four unjittered Es are the templates to be matched to the jittered data. The first model that we considered calculated the likelihood of the 17! possible correspondences between the jittered data and the four templates. There were too many possible correspondences to do the calculation. The present model calculates the likelihood, treating each sample independently. Consider the jth jittered sample. Because of the jitter, one doesn't know what its original location was. For this model we sum up the likelihoods that the datum came from each of the 17 possible locations, T_{ki} for the given template.

$$L_{kj} = \sum_{i=1}^{17} \exp(-((T_{kix} - D_{jx})^2 + (T_{kix} - D_{jy})^2)/2\sigma^2) \quad (4)$$

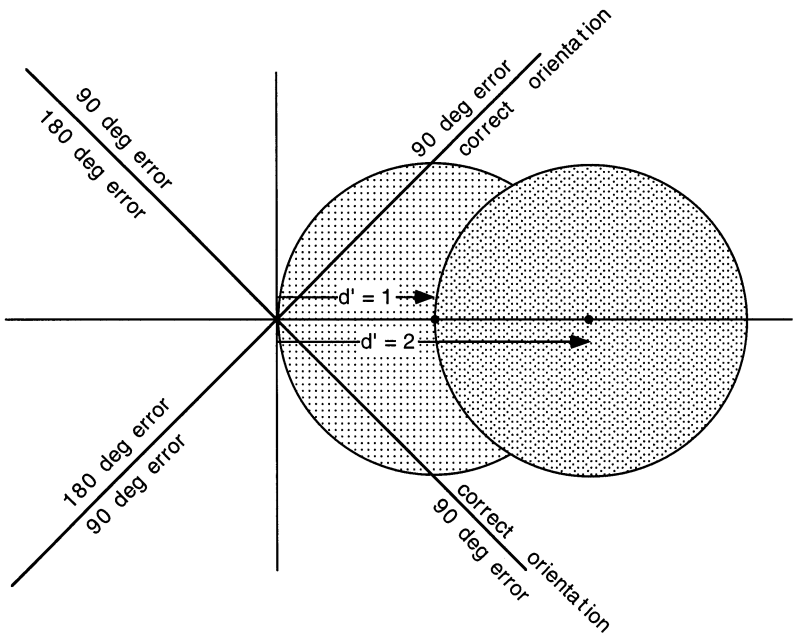

Fig. 13. Schematic of the Gaussian asymmetry model. The abscissa and ordinate represent the amounts of horizontal and vertical asymmetry respectively. The circles represent one standard deviation of the asymmetry centered at a distance of 1 and 2 units on the abscissa. The two diagonal lines through the origin represent the decision boundaries. When the asymmetry lies in the right hand quadrant the letter is judged to be in the correct orientation. When it lies in the upper or lower quadrants the letter is misjudged by 90° and when it is in the left quadrant a 180° error is made.

where the template and data locations are specified just as they were in model 1. The likelihood inside the summation is identical to that in Eq. (1). The only difference is that the index i is now independent of index j. The total likelihood of the kth orientation is the product of the likelihoods of each of the 17 data samples. Equivalently, one can refer to the log likelihood, LL, in which case the total log likelihood is a sum over the individual log likelihoods:

$$LL_k = \sum_{j=1}^{17} \log(L_{kj}) \tag{5}$$

Finally, the decision about which orientation to choose is based on which of the four log likelihoods in Eq. (5) is maximal. The output of this model is shown in Fig. 12A and B.

A.2.3. Model 3: Separable signal detection model—Gaussian asymmetry

We wanted to test a filter model that could indicate the orientation of the E. The asymmetry model we used is one version of such a filter model (the notion of a filter model is that one does a weighted average over the stimulus and arrives at a single decision variable). The 17 samples that are used to represent a vertical E, are distributed symmetrically in the vertical direction but asymmetrically in the horizontal direction. This horizontal asymmetry, A, can be used to identify the orientation of the E. When the samples are jittered, the asymmetry will be noisy, causing errors. The model to be examined in this section makes the assumption that the asymmetry noise, n_A, has Gaussian variability that is equal in the horizontal and vertical directions. In that case an analysis similar to that of Fig. 2 of Klein (1985) can be carried out as shown in our Fig. 13. The abscissa and ordinate represent the amounts of horizontal and vertical asymmetry. The circles represent one standard deviation of the asymmetry centered at a distance of 1 and 2 units on the abscissa. The two diagonal lines through the origin represent the decision boundaries. When the asymmetry lies in the right hand quadrant the E-pattern is judged to be in the correct orientation. When it lies in the upper or lower quadrants the E-pattern is misjudged by 90° and when it is in the left quadrant a 180° error is made.

The probability of lying in the righthand quadrant ($\text{prob}_{\text{correct}}$) is equal to the product of the probabilities of being to the right of both of the diagonal lines (because of the separability of the bivariate Gaussian distribution).

$$\text{prob}_{\text{correct}} = P^2 \tag{6}$$

where

$$p = \int_{-\infty}^{z} \exp(-x^2/2)\,\mathrm{d}x \tag{7}$$

and

$$z = d'/2^{1/2} \tag{8}$$

The connection between P and z is the standard connection between probability and z-score. The sqrt(2) factor arizes because the distance from the center of the asymmetry distribution to one of the diagonal lines equals d' cos(45°).

The d' value is the distance from the origin to the center of the asymmetry distribution in units of the noise standard deviation.

$$d' = \mathrm{A}/n_{\mathrm{A}} \tag{9}$$

From Fig. 13 it is seen that the probability of lying in the upper or lower quadrants (the probability of making a 90° error) is

$$\mathrm{prob}_{90} = P(1-P) \tag{10}$$

Finally, the probability of being in the lefthand quadrant is:

$$\mathrm{prob}_{180} = (1-P)^2 \tag{11}$$

The three probabilities must add up to unity (with prob_{90} being counted twice):

$$\mathrm{prob}_{\mathrm{correct}} + 2\ \mathrm{prob}_{90} + \ \mathrm{prob}_{180} = 1 \tag{12}$$

Fig. 14A plots the two error probabilities, prob_{90} and prob_{180}. We have chosen to plot prob_{90} rather than 2*prob_{90} (which was used in Figs. 11 and 12) in order to simplify the comparison to prob_{180}. For the top panel the data has been plotted with the abscissa chosen to be $1/d'$. The quantity $1/d'$ is roughly proportional to the magnitude of sample jitter (Eq. (9)), so the bottom panel might be expected to resemble Figs. 11 and 12. For large values of noise, both the 90° and 180° errors approach 25%, as would be expected from guessing. The noteworthy aspect of Fig. 14A is that the 180° errors grow very slowly with asymmetry noise. Thus when the 90° errors have reached 23% the 180° errors are only 13%. This comparison is important in two regards: (1) for the human data the two types of errors are much closer together (see Fig. 12A); therefore this general class of models can be excluded; (2) this pattern of predicted 90° and 180° errors is reversed from the undersampling case shown in Fig. 14B, where the 90° errors are much less than the 180°.

By plotting prob_{90} as a function of prob_{180} in Fig. 12A, the dependence on the amount of jitter has been eliminated. From Eqs. (10) and (11), the signal detection asymmetry model predicts a simple connection between the two probabilities:

$$\mathrm{prob}_{90} = 2(\mathrm{sqrt}(\mathrm{prob}_{180}) - \mathrm{prob}_{180}) \tag{13}$$

Eq. (13) is plotted as the solid curve in Fig. 12A.

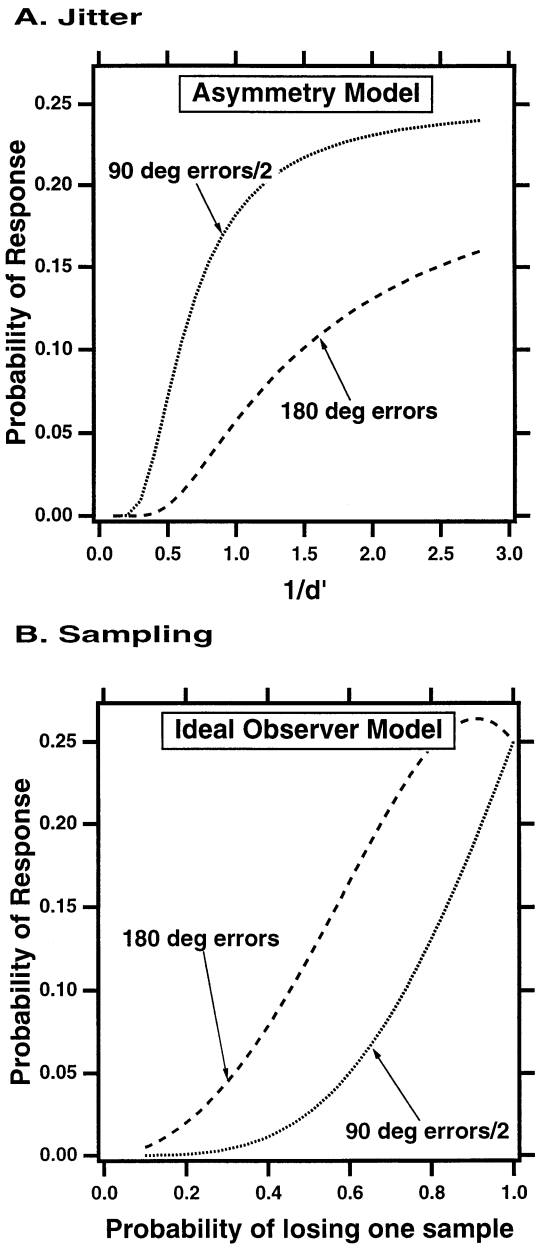

Fig. 14. Two error probabilities, prob_{90} and prob_{180}: (A). For the Gaussian jitter asymmetry model. The abscissa is $1/d'$, which is roughly proportional to the magnitude of sample jitter (Eq. (9)). Note that the 180° errors grow very slowly with asymmetry noise, and do not mimic the human errors (see Fig. 12A); therefore this general class of models can be excluded. Also, this pattern of predicted 90° and 180° errors is reversed from the undersampling case shown in Fig. 14B, where the 90° errors are much less than the 180° errors. (B). For the ideal observer model. The abscissa is the probability of losing one sample. (Note that errors of the asymmetry model are much closer together).

References

Artal, P., Derrington, A. M., & Colombo, E. (1995). Refraction, aliasing, and the absence of motion reversals in peripheral vision. *Vision Research*, *35*, 939–947.

Baker, F. H., Grigg, P., & von Noorden, G. K. (1974). Effects of visual deprivation and strabismus on the responses of neurons in the visual cortex of the monkey, including studies on the striate and prestriate cortex in the normal animal. *Brain Research*, *66*, 185–208.

Bradley, A., & Freeman, R. D. (1981). Contrast sensitivity in anisometropic amblyopia. *Investigative Ophthalmology and Visual Science*, *21*, 467–476.

Fahle, M., & Bachmann, G. (1996). Better performance through amblyopic than through normal eyes. *Vision Research*, *36*, 1939–1996.

Feldman, J. (1997). Curvilinearity, covariance, and regularity in perceptual groups. *Vision Research*, *37*, 2835–2848.

Field, D. J., & Hess, R. F. (1996). Uncalibrated distortions versus undersampling. *Vision Research*, *36*, 2121–2124.

Field, D. J., Hayes, A., & Hess, R. F. (1993). Contour integration by the human visual system: evidence for a local 'association field'. *Vision Research*, *33*, 173–193.

Geisler, W. S. (1989). Sequential ideal-observer analysis of visual discriminations. *Psychology Review*, *96*, 267–314.

Hess, R. F., & Anderson, S. J. (1993). Motion sensitivity and spatial undersampling in amblyopia. *Vision Research*, *33*, 881–896.

Hess, R. F, & Field, D. J. (1993). Is the increased spatial uncertainty in the normal perihery due to spatial undersampling or uncalibrated disarray? *Vision Research*, *33*, 2663–2670.

Hess, R. F., & Field, D. (1994). Is the spatial deficit in strabismic amblyopia due to loss of cells or an uncalibrated disarray of cells? *Vision Research*, *34*, 3397–3406.

Hess, R. F., & Howell, E. R. (1977). The threshold contrast sensitivity function in strabismic amblyopia: evidence for a two-type classification. *Vision Research*, *17*, 1049–1055.

Hess, R. F., & McCarthy, J. (1994). Topological disorder in peripheral vision. *Visual Neuroscience*, *11*, 1033–1036.

Hess, R. F., & Watt, R. J. (1990). Regional distribution of the mechanisms that underlie spatial localization. *Vision Research*, *30*, 1021–1031.

Hess, R. F., Campbell, F. W., & Greenhalgh, T. (1978). On the nature of the neural abnormality in human amblyopia: neural aberrations and neural sensitivity loss. *Pfluegers Archivs*, *377*, 201–207.

Hess, R. F., McIlhagga, W., & Field, D. J. (1997). Contour integration in strabismic amblyopia: the sufficiency of an explanation based on positional uncertainty. *Vision Research*, *37*, 3145–3161.

Imamura, K., Richter, H., & Fischer, H. (1997). Reduced activity in the extrastriate visual cortex of individuals with strabismic amblyopia. *Neuroscience Letters*, *225*, 173–176.

Klein, S. A. (1985). Double-judgment psychophysics: problems and solutions. *Journal of the Optical Society of America A*, *2*, 1560–1585.

Koenderink, J. J., Bouman, M. A., & Bueno de Mesquita, A. E. (1978). Perimetry of contrast detection thresholds of moving sine wave patterns. *Journal of the Optical Society of America A*, *68*, 845–865.

Levi, D. M., & Harwerth, R. S. (1977). Spatio-temporal interactions in anisometropic and strabismic amblyopia. *Investigative Ophthalmology and Visual Science*, *16*, 90–95.

Levi, D. M., & Klein, S. (1985). Vernier acuity, crowding and amblyopia. *Vision Research*, *25*, 979–991.

Levi, D. M., & Klein, S. A. (1986). Sampling in spatial vision. *Nature*, *320*, 360–362.

Levi, D. M., & Klein, S. A. (1992). Weber's law' for position: the role of spatial frequency and contrast. *Vision Research*, *32*, 2235–2250.

Levi, D. M., & Klein, S. A. (1996). Limitations on position coding imposed by undersampling and univariance. *Vision Research*, *36*, 2111–2120.

Levi, D. M., & Sharma, V. (1998). Integration of local orientation in strabismic amblyopia. *Vision Research*, *38*, 775–781.

Levi, D. M., & Waugh, S. J. (1994). Spatial scale shifts in peripheral vernier acuity. *Vision Research*, *34*, 2215–2238.

Levi, D. M., Klein, S. A., & Aitsebaomo, A. P. (1985). Vernier acuity, crowding and cortical magnification. *Vision Research*, *25*, 963–977.

Levi, D. M., Sharma, V., & Klein, S. A. (1997). Feature integration in pattern perception. *Proceedings of the National Academy of Science of the United States of America*, *94*, 11742–11746.

Levi, D. M., Klein, S. A., & Wang, H. (1994a). Amblyopic and peripheral vernier acuity: a test-pedestal approach. *Vision Research*, *34*, 3265–3292.

Levi, D. M., Klein, S. A., & Wang, H. (1994b). Discrimination of position and contrast in amblyopic and peripheral vision. *Vision Research*, *34*, 3293–3314.

Levi, D. M., Klein, S. A., & Yap, Y. L. (1987). Positional uncertainty in peripheral and amblyopic vision. *Vision Research*, *27*, 581–597.

Levi, D. M., Waugh, S. J., & Beard, B. L. (1994). Spatial scale shifts in amblyopia. *Vision Research*, *34*, 3315–3334.

Parish, D. H., & Sperling, G. (1991). Object spatial frequencies, retinal spatial frequencies, noise and the efficiency of letter discrimination. *Vision Research*, *31*, 1399–1415.

Polat, U., & Sagi, D. (1993). Lateral interactions between spatial channels: suppression and facilitation revealed by lateral masking experiments. *Vision Research*, *33*, 933–999.

Polat, U., & Sagi, D. (1994). The architecture of spatial interactions. *Vision Research*, *34*, 73–78.

Rovamo, J., Virsu, V., & Nasanen, R. (1978). Cortical magnification factor predicts photopic contrast sensitivity of peripheral vision. *Nature London*, *271*, 54–56.

Saarinen, J., Levi, D. M., & Shen, B. (1997). Integration of local pattern elements into a global shape in human vision. *Proceedings of the National Academy of Science of the United States of America*, *94*, 8267–8271.

Sharma, V., Levi, D. M., & Coletta, N. J. (1997). Sparse sampling in central vision of strabismic amblyopes. *Investigative Ophthalmology and Visual Science*, *38*, 108.

Solomon, J. A., & Pelli, D. G. (1994). The visual filter mediating letter identification. *Nature*, *369*, 395–397.

Virsu, V., & Rovamo, J. (1979). Visual resolution, contrast sensitivity, and the cortical magnification factor. *Experimental Brain Research*, *37*, 475–494.

Wang, H., Levi, D. M., & Klein, S. A. (1998). Spatial uncertainty and sampling efficiency in amblyopic position acuity. *Vision Research*, *38*, 1239–1251.

Wang, Y. Z., Thibos, L. N., & Bradley, A. (1996). Undersampling produces non-veridical motion perception, but not necessarily motion reversal, in peripheral vision. *Vision Research*, *36*, 1737–1744.

Watson, A. B. (1987). Estimation of local spatial scale. *Journal of the Optical Society of America A*, *4*, 1579–1582.

Watt, R. J., & Hess, R. F. (1987). Spatial information and uncertainty in anisometropic amblyopia. *Vision Research*, *27*, 661–674.

Wiesel, T. N. (1982). Postnatal development of the visual cortex and the influence of environment. *Nature*, *299*, 583–591.

Wilson, H. R. (1991). Model of peripheral and amblyopic hyperacuity. *Vision Research*, *31*, 967–982.